Nature Communications

https://doi.org/10.1038/s41467-026-75078-6

Article in Press

Visible Light-Induced Intermolecular Dearomatization for Constructing Angularly Fused Tetracyclic Scaffolds

Received: 24 September 2025

Accepted: 15 June 2026

Published online: 30 June 2026

Cite this article as: Lin, F., Song, T.-T., Zhang, L.-M. *et al.* Visible Light-Induced Intermolecular Dearomatization for Constructing Angularly Fused Tetracyclic Scaffolds. *Nat Commun* (2026). https://doi.org/10.1038/s41467-026-75078-6

Fan Lin, Ting-Ting Song, Li-Ming Zhang, Zhi-Yuan Ding, Yilitabaier Julaiti, Yanhua Lu, Boshun Wan, Yaguang Sun & Qing-An Chen

Visible Light-Induced Intermolecular Dearomatization for Constructing Angularly Fused Tetracyclic Scaffolds

Fan Lin,[1,2] Ting-Ting Song,*[,1] Li-Ming Zhang,[1,3] Zhi-Yuan Ding,[1,3] Yilitabaier Julaiti,[1,3] Yanhua Lu,[4] Boshun Wan,[1,3] Yaguang Sun,*[,2] Qing-An Chen*[,1,3]

[1]Dalian Institute of Chemical Physics, Chinese Academy of Sciences, 457 Zhongshan Road, Dalian 116023, China
[2]Shenyang University of Chemical Technology, Shenyang 110142, China
[3]University of Chinese Academy of Sciences, Beijing 100049, China
[4]Hubei Institute of Aerospace Chemotechnology, Xiangyang, 441003, China
*Corresponding author: E-mail: ttsong@dicp.ac.cn, sunyaguang@syuct.edu.cn, qachen@dicp.ac.cn

Abstract

Visible light-induced dearomative cycloaddition has emerged as a powerful strategy for constructing complex polycyclic frameworks from simple aromatic precursors. Angularly fused polycyclic systems, which exhibit distinctive structural rigidity and tunable physicochemical properties, represent privileged scaffolds in bioactive natural products and pharmaceuticals. Herein, we report a robust photocatalytic protocol for the direct assembly of angularly fused tetracyclic scaffolds through intermolecular dearomatization of benzothiophene/indole derivatives with *N*-aryl cyclopropylamines. This transformation is achieved via a mechanistically intriguing cascade involving photocatalytic dearomative [3+2] cycloaddition and subsequent cyclization. This work demonstrates the synthetic feasibility of photocatalytic intermolecular dearomative [3+2] processes, providing direct access to structurally distinct angularly fused tetracyclic cores.

Introduction

Characterized by their distinct three-dimensional architectures, angularly fused polycyclic scaffolds represent a privileged structural motif in bioactive natural products and pharmaceuticals with diverse biological activities (Fig. 1a)[1,2]. As a natural indole alkaloid, strychnine has been used as a potent rodenticide due to its potent neurotoxic activity mediated through glycine receptor antagonism in the central nervous system[3,4]. The monoterpene indole alkaloid aspidospermidine demonstrates dual pharmacological activities as both a respiratory stimulant and antimicrobial agent[5]. Schizozygine, a bioactive alkaloid from schizozygia caffaeoides, shows antimicrobial effects relevant to its traditional dermatological applications[6]. Similarly, alstonlarsine A has been identified as a selective DRAK2 kinase inhibitor with therapeutic potential[7]. Therefore, the construction of angularly fused tetracyclic scaffolds is of great interest.

Over the past decade, visible light-induced dearomative cycloadditions[8-16], have emerged as a powerful strategy for the expedient synthesis of strained polycyclic architectures[17-24,25-28,29] that are challenging to access through traditional methods. Particularly, You[30-33], Oderinde[34], and other groups[35-39] have demonstrated pioneering work showing that triplet-state electron-deficient indoles readily engage in intramolecular dearomative [2+2], [4+2], and [5+2] cycloadditions to construct diverse angularly fused polycyclic scaffolds via an energy transfer mechanism (Fig. 1b). Among these, only one case involving a single electron transfer process was reported by Yang et al[40]. While intramolecular variants have been well-explored, the development of intermolecular dearomative cycloadditions–especially those forming angularly fused systems–remains underexplored and represents a significant synthetic challenge.

Meanwhile, cyclopropylamine (CPA) derivatives have emerged as intriguing synthons in modern organic synthesis, particularly for the construction of valuable cyclic amines[41-43]. Their synthetic utility stems from a characteristic ring-opening pathway initiated by single-electron oxidation to form reactive nitrogen radical cations (Fig. 1c)[41]. This distinctive reactivity enables CPAs to participate in cycloadditions with alkenes[44-50], alkynes[51,52], or bicyclo[1.1.0]butanes[53], providing efficient access to structurally diverse cyclic amine scaffolds. Inspired by these precedents and based on our research interests in photocatalytic dearomatization[54-57], we envisioned that combining the photochemical excitation of benzothiophenes or indoles with the radical reactivity of *N*-aryl cyclopropylamines could enable distinctive dearomative cycloadditions (Fig. 1d). In this context, it is challenging to suppress the self-dimerization of aromatic compounds without disturbing photocatalysis. The design of the substrates and the selection of the photosensitizer are critical factors in the transformation process. Herein, we developed a robust photocatalytic protocol for the direct assembly of angularly fused tetracyclic scaffolds through intermolecular dearomatization of benzothiophene/indole derivatives with *N*-aryl cyclopropylamines (Fig. 1e). This protocol not only expands the toolbox for dearomatization but also provides rapid access to complex heterocycles relevant to medicinal chemistry and materials science.

Results and Discussion

The evaluation of reaction conditions commenced with methyl benzothiophene-2-carboxylate (**1a**) and *N*-phenyl cyclopropylamine (**2a**) as the model substrates (Table 1, see Supplementary Information for details). Pleasingly, under blue LEDs irradiation for 20 h, the saturated bicyclic amine **4a** could be obtained in 50% yield with $[Ir(dF(CF_3)_2bbpy)(ppy)_2]PF_6$ (**PC-I**, 1 mol%) in acetone (0.1 M) (entry 1), accompanied by the inevitable formation of dimer (**3a**) of **1a**. Dimer **3a** was obtained with high diastereoselectivity (> 95:5), and the absolute configuration was unambiguously assigned by single-crystal X-ray diffraction (CCDC: 2526038). In addition, both diastereomers of the [3+2] cycloadduct **4a** (*trans*) and **4a'** (*cis*) were successfully isolated. The configuration of **4a'** (*cis*) was also confirmed

by single-crystal X-ray diffraction (CCDC: 2526040). Screening of solvents revealed that THF and DCM resulted in relatively low yields (entries 1–3). Photosensitizers $[Ir(ppy)_2(dtbbpy)]PF_6$ (**PC-II**), $Ir(dFppy)_2(pic)$ (**PC-III**), TXT (**PC-IV**), and 5CzBN (**PC-V**) proved to be less efficient (entries 4–7). Yet, through extensive conditional optimization, attempts to suppress dimerization failed (Please see Supplementary Tables 1–4 for details). The control experiments with the isolated compounds **4a** (*trans*) and **4a'** (*cis*) demonstrated that none of the tested conditions (e.g. photocatalysis, thermal activation, or base promotion) facilitated their cyclization to the lactam **5a**. Instead, under either photochemical or basic conditions, **4a** (*trans*) and **4a'** (*cis*) underwent mutual isomerization to establish an equilibrium (Please see Supplementary Tables 22 and 23 for details). This impasse highlighted the need for a more reactive acylating reagent capable of driving the cascade to completion. We therefore pivoted to a substrate-design strategy, hypothesizing that kinetically accelerating the [3+2] step could outcompete dimerization. Inspired by precedents employing pyrazole derivatives as superior leaving groups in dearomative photocycloadditions[14,20,29], we evaluated a series of benzothiophene substrates bearing acyl pyrazoles (entries 8–12). Gratifyingly, all such substrates successfully delivered product **5a**, confirming the activated group's role as an integral "cyclization driver." Notably, when bulky aryl substituents were introduced on the pyrazole moiety, the formation of the dimer could be effectively suppressed. In particular, the phenyl-substituted substrate afforded the target product **5a** in an isolated yield of 71%. Corresponding [3+2] cycloadduct **4d'** (*cis*) could be isolated in other solvent systems (DMSO or $MeNO_2$, entries 13 and 14), whose configuration was similarly established by single-crystal X-ray diffraction (CCDC: 2526041). Finally, control experiments established the indispensability of both light and the photocatalyst (entries 15 and 16).

With the optimized reaction condition established, we investigated the scope of aromatic substrates and *N*-aryl cyclopropylamines (Fig. 2). First, substitutions on the *N*-aryl cyclopropylamines were evaluated. Pleasingly, the *para*-substituted *N*-aryl cyclopropylamines bearing various electron-donating groups (-Me, -^{t}Bu, and -OMe) performed well, affording the products (**5b**–**5d**) in 56–68% yields. In addition, angularly fused polycyclic products (**5e**–**5g**) with electron-withdrawing substituents could also be obtained in a reasonable yield. The -OMe group at the *meta* position of the arylamine was also applicable in this protocol, affording the desired product **5h**. Furthermore, 2-substituted *N*-aryl cyclopropylamines performed well, delivering polycyclic products (**5i** and **5j**) in high yields. The pyridyl, 1-naphthyl, and 2-naphthyl groups could also be tolerated in this strategy (**5k**–**5m**). Furthermore, *N*-aryl cyclobutylamines bearing various groups have also been explored. The [4+2] cycloaddition reaction generally tolerated both electron-donating (-^{t}Bu, -OMe, and $-OCF_3$) substituents on the aryl ring, forming angularly fused tetracyclic products (**5n**–**5q**) in 60–69% yields. However, attempts to employ other known cyclopropanamine precursors, such as *N*-tosyl cyclopropylamines[58] or *N*-cyclopropylureas[59] under the developed conditions proved unsuccessful (Please see Supplementary Tables 11–14 for details).

Next, we examined the scope of benzothiophenes for this dearomative cycloaddition reaction. The 5-position Me-substituted benzothiophene substrate worked smoothly, thus providing polycyclized product **5r**. Then, the applicability of aromatic substrates bearing various electron-withdrawing groups (-X and -CF_3) at the 5-position was further investigated. The desired products **5s**–**5v** could also be accessed in 53–62% yields. The 5-methoxy-substituted substrate underwent successful transformation, yielding the desired product **5w**. Moreover, naphthyl as well as heterocyclic substituents such as pyrrole and thiophene were well tolerated in this dearomative cycloaddition (**5x**–**5z**). Substrates with electron-withdrawing groups at the 6-position of the phenyl ring were likewise compatible with this protocol (**5aa** and **5ab**). The structure of **5ab** was further confirmed by single-crystal X-ray crystallography (CCDC: 2468281). The reaction proceeded efficiently with 7-substituted benzothiophenes, affording products **5ac** and **5ad**. Benzothiophene with chlorine at the 4-position was successfully converted to the product **5ae** in moderate yield.

Furthermore, substituted benzothiophenes (-Me and -F) participated readily in the reaction with *N*-Ph cyclobutylamine, delivering target products (**5af** and **5ag**) in good yields. The structures of **5ad** and **5af** were further confirmed by single-crystal X-ray crystallography (CCDC: 2526042 and 2468282). A naproxen-derived benzothiophene also underwent smooth cycloaddition with *N*-phenyl cyclopropylamine to deliver the target compound **5ah**. These results collectively demonstrate that the electronic nature of the substituent is not a limiting factor for this transformation, with both electron-donating and -withdrawing groups being well tolerated. However, C2-substituted benzofuran substrates proved incompatible with our developed photocatalytic protocol (Please see Supplementary Tables 8–10 for details). We attribute the lack of reactivity with benzofuran substrates to their unfavorable electronic properties. Even with an electron-withdrawing acyl pyrazole at C2, the strong π-donating ability of oxygen in benzofuran keeps the C2=C3 bond insufficiently electrophilic, which hinders its reaction with nucleophilic radical species, leading to low reactivity.

Subsequently, substrate scope of the dearomative reaction from the indoles and *N*-aryl cyclopropylamines was investigated (Fig. 3a). Initial study with **6a** was carried out to provide the corresponding product **7a** in 73% isolated yield. Notably, the addition of Et_3N is necessary to facilitate diastereomeric interconversion, thereby enabling more efficient elimination of the pyrazole moiety and subsequent cyclization. A variety of substituents on the phenyl ring of *N*-aryl cyclopropylamines, including -Me, -OMe, and -F, were well-tolerated, delivering desired products (**7b**–**7d**) in reasonable yields. The structure of **7c** was further confirmed by single-crystal X-ray crystallography (CCDC: 2468232). Moreover, the 5-bromoindole substrate underwent the reaction smoothly, affording angularly fused tetracyclic product **7e**. The 6-bromo-substituted product **7f** was also successfully isolated by subjecting the intermediate formed in the previous step to continued irradiation at 390 nm. In the reaction with *N*-phenylcyclobutane, the [4+2] cycloaddition product could not be isolated when acetone was used as the reaction solvent. Instead, an interesting tetrahydrofuran-involved

hydroalkylation product **7g'** was obtained (THF as solvent). The structure of **7g'** was further confirmed by single-crystal X-ray crystallography (CCDC: 2526043). This transformation likely proceeds via a photo-promoted hydrogen atom transfer (HAT) process, followed by reaction with alkyl radical (from THF) to afford the dearomative hydroalkylation product. Notably, the unprotected indole substrate **6h** failed to react. This is likely because the strong π-donation from the unprotected N–H (*vs* electron-withdrawing Boc group) indole nitrogen excessively enriches the C2=C3 bond, reducing its electrophilicity and hindering productive reaction with a nucleophilic radical partner. To our delight, benzothiophene and benzofuran with an acyl pyrazole group at the 3-position proved amenable to this protocol, yielding the corresponding angularly fused tetracyclic products **7i** and **7j**. To further delineate the structural requirements for this transformation, we examined a variety of heterocyclic substrates beyond the successful 2-acylpyrazole-substituted benzothiophenes and *N*-Boc-protected 3-acylpyrazole-substituted indoles. As illustrated in Supplementary Fig. 2, *N*-methylindole, thiophene, and coumarin derivatives all exhibited poor reactivity. In other cases, such as with substrates containing methyl esters (CO_2Me) at distinct positions, the reactions were sluggish. These unsuccessful attempts are compiled in the Supplementary Information to provide a complete picture of the reaction scope and limitations.

Without presynthesizing acyl pyrazole in advance, we successfully developed a one-pot synthetic strategy that enabled the direct conversion of benzothiophene-2-carboxylic acids into angularly fused tetracyclic products (Fig. 3b). This further highlights the versatility and mild reaction conditions of our protocol. When employing thianaphthene-carboxylic acid as the substrate, various *N*-aryl cyclopropylamines underwent smooth transformation to afford the corresponding products (**5a**, **5b**, **5d**, **5e**, and **5n**). Furthermore, substituted benzothiophene-2-carboxylic acids also proved to be suitable substrates for this transformation through in situ activation of the carboxylic acid group, as demonstrated by the successful synthesis of compounds **5r**, **5s**, and **5y**.

To shed light on our mechanistic hypothesis, a series of mechanistic experiments were conducted (Fig. 4). First, when **1ai** was subjected to the standard reaction conditions, no target product was produced, ruling out the possibility of **1ai** being a reaction intermediate (Fig. 4a). Second, the kinetic profile of a standard reaction mixture of **1d** and **2a** showed that the reaction proceeded very rapidly and did not have obvious induction periods, with the majority of the product formed within 5 h (Fig. 4b). Next, light on/off experiments demonstrated that the transformation was interrupted in the absence of light (Fig. 4c). It suggests the crucial role of light irradiation and rules out a long radical chain process. Moreover, the photocatalyst **PC-1** was found to be the only light-absorbing species in the reaction near the excitation wavelength from ultraviolet–visible (UV-vis) absorption spectroscopy (Fig. 4d). Then, Stern−Volmer luminescence quenching experiments were performed using **1d**, **2a**, and **6a**, respectively (Fig. 4e). The results demonstrate that both substrate **1d** and cyclopropylamine **2a** are competent quenchers of the excited photocatalyst **PC-I***, with **1d** exhibiting significantly higher quenching efficiency than **2a**. It implies that the intertwined EnT/SET or SET pathway is likely

involved in the formation of **5**. While no obvious quenching was observed for indole **6a**, this indicates that radical addition is involved in the formation of **7**.

The dearomative process was suppressed when adding radical inhibitors TEMPO or BHT (Fig. 4f, entries 1–3), which suggests the reaction proceeds via a radical mechanism. And the observation of TEMPO-adduct by ESI-HRMS suggests that the radical intermediate is likely involved in the reaction. On the other hand, the standard reaction was significantly inhibited in the presence of known triplet quenchers, such as O_2 or 1,1-diphenylethylene (Fig. 4f, entries 4 and 5). When using 2,5-dimethylhexa-2,4-diene as a diradical scavenger under standard conditions, the [2+2] adduct [**8a** + **8a'**] was detected and isolated in 46% yield (Fig. 4g). The structure of **8a** was confirmed by single-crystal X-ray crystallography (CCDC: 2526044). The detection of a diradical intermediate provides evidence for the involvement of triplet-state species, suggesting that an energy transfer mechanism may be involved in this dearomatization process. To understand the nature of the reaction, the $\Delta G(T_1-S_0)$ values of substrates **1a** (55.8 kcal mol^{-1}), **1d** (54.4 kcal mol^{-1}), and **6a** (59.6 kcal mol^{-1}) were calculated. As a result, the yield of corresponding product did not exhibit a straightforward linear dependence on the triplet energy of photocatalysts (Supplementary Table 2). In addition, electrochemical studies also show that it is thermodynamically feasible for the excited photocatalyst ($E_{p/2}^{III*/II}$ = +1.21 V vs SCE in CH_3CN) to oxidize substrate **2a** ($E_{p/2}^{ox}$ = +1.19 V vs SCE in CH_3CN) via SET (Supplementary Fig. 10)[41,44,60]. However, for substrates **1d** ($E_{p/2}^{ox}$ = +0.75 V, +1.86 V, and $E_{p/2}^{red}$ = -1.12 V, -1.52 V vs SCE in CH_3CN) and **6a** ($E_{p/2}^{ox}$ = +1.82 V, and $E_{p/2}^{red}$ = -1.10 V, -1.85 V vs SCE in CH_3CN), no obvious correlation between the oxidation/reduction potentials and the reactivity was found. For the indole substrate **6a**, the addition of NEt_3 led exclusively to the formation of the *trans*-configuration [3+2] cycloadduct **7aa** (*trans*). In the absence of the base, both diastereomers **7aa** (*trans*) and **7aa'** (*cis*) were isolated successfully with 64:36 dr (Fig. 4h). In addition to routine NMR analysis, variable-temperature ^1H NMR experiments were performed to assess the conformational stability of both compounds (**7aa** and **7aa'**) (Supplementary Figs. 12 and 13). Control experiments demonstrated that both **7aa** (*trans*) and **7aa'** (*cis*) could be converted to the target product **7a** under base-promoted conditions. Under photochemical conditions, conversion of **7aa** (*trans*) was inhibited in the presence of NEt_3 (Supplementary Table 27). However, under prolonged irradiation in the absence of NEt_3, **7aa** (*trans*) was efficiently transformed into lactam **7a**. Short-term monitoring of the photochemical process revealed an initial formation of the *cis*-isomer **7aa'** (*cis*) (Fig. 4i, eq. 1). Furthermore, the *cis*-configuration pyrazole-substituted adducts **4d'** (*cis*) or **7aa'** (*cis*) were efficiently transformed into lactam **5a** or **7a** via either photochemical or base-mediated pathways (Fig. 4i, eq. 2 and 3). Collectively, these results provide compelling evidence that the *trans*-configuration [3+2] cycloadducts first undergo isomerization to their *cis*-counterparts, which subsequently serve as the direct precursors for the final cyclization step to afford the desired lactam products (**5** or **7**).

Based on DFT calculations and mechanistic experiments, a plausible mechanism is postulated as outlined (Fig. 5, please see Supplementary Information and Source Data for details). First, visible light excitation of the photocatalyst yields an excited state complex which sensitizes **1d** via the EnT process, affording diradical intermediate **A**. Radical addition of species **A** to substrate **1d** furnishes intermediate **B**. Subsequent intramolecular radical-radical coupling of **B** leads to the undesired dimer **3d**. In the meantime, the photoexcited species $\mathbf{Ir^{III}*}$ undergoes a single-electron reduction by cyclopropylamine (**2a**) to deliver $\mathbf{Ir^{II}}$ and radical cation species **C**. A subsequent ring opening via *β*-scission delivers distonic radical cation **D**. Next, radical addition with **1d** with radical cation species **D** (path I) furnishes another distonic radical cation **E**. The direct combination of two relatively low-concentration excited-state species (**A** and **D**, path II) is kinetically unlikely. Subsequently, species **E** undergoes cyclization, providing access to the radical cation **F**. At this stage, **F** could be reduced by the $\mathbf{Ir^{II}}$ species generated in the reductive quenching photoredox cycle, delivering [3+2] cycloadducts *trans*-**G** and *cis*-**G**. At the same time, the alternative pathway (path III: reduction–direct cyclization) remains a possibility.

The target angular-fused lactam **5a** can be generated through two distinct pathways (photo-induced or base-promoted pathway, Fig. 5). Under photo-induced conditions, the carbonyl group of *trans*-**G** is photoexcited to generate the diradical species *trans*-**H**, which then undergoes *β*-scission via transition state *trans*-**TS5** to afford intermediate **I**. Subsequent radical addition yields the excited-state species *cis*-**J**, thereby achieving configurational inversion. The species *cis*-**J** can also originate from the excitation of the *cis*-**G**. Intermediate *cis*-**J** undergoes a 1,5-H transfer to form *cis*-**K**, which further cyclizes to give intermediate **L**. Subsequent deprotonation followed by pyrazole elimination affords the target product **5a**. In an alternative pathway, intermediate *trans*-**G** undergoes deprotonation under basic conditions (DBU) to generate the anionic intermediate *trans*-**N**. The elimination (retro-Mannich reaction) of *trans*-**N** affords ring-opening species **O** via transition state *trans*-**TS7** (with an activation energy of 13.2 kcal mol^{-1}), thereby achieving racemization of the stereocenter next to the sulfur atom. A subsequent addition partially yields the *cis*-configured intermediate *cis*-**N**, which can also be afforded from *cis*-**G** in the presence of DBU. The anionic *cis*-**N** then undergoes addition–cyclization onto the carbonyl group to form intermediate **M**, followed by pyrazole elimination to furnish the desired lactam **5a**. Additionally, computational results indicate that, compared to the acylpyrazole-substituted substrate **1d**, the intermediate *cis*-$\mathbf{N_{1a}}$ derived from the methyl formate-substituted substrate **1a** needs to overcome a higher energy barrier (9.4 kcal mol^{-1}) in the subsequent cyclization step (*cis*-$\mathbf{N_{1a}}$ to $\mathbf{M_{1a}}$). Moreover, due to the stronger nucleophilicity of the OMe, which makes it a poorer leaving group, 3+2 cyclization product **4a** is a thermodynamically stable product (Supplementary Fig. 37).

To further demonstrate the synthetic potential of this protocol, we carried out scale-up synthesis of angularly fused polycyclic products (**5a** and **7a**) under standard conditions, and the efficiencies did not erode significantly (Fig. 6a).

These compounds serve as versatile building blocks, enabling further structural diversification through subsequent transformations (Fig. 6b). Initially, with the addition of $LiAlH_4$, β-lactam **5a** could be reduced to yield azetidine **9** in 62% yield. Subsequently, oxidation of azetidine **9** with *m*CPBA yielded the corresponding sulfoxides **10** and **10'**, with concurrent azetidine ring opening. This ring cleavage, likely driven by ring strain release or nucleophilic attack-induced C–N bond cleavage, resulted in the formation of N-phenyl amino alcohol. Furthermore, sulfone **11** was created from **9** through further oxidation with H_2O_2. X-ray structures of products **10**, **10'**, and **11** were presented to confirm their configurations (CCDC: 2473229–2473231). The chemoselective oxidation of **5a** by CAN was successfully carried out to give sulfoxides **12** and **12'** in 80% total yield with 4:1 diastereoselectivity due to the chirality of sulfur. Oxidative amidation of sulfoxide **12** with hypervalent iodine reagent could afford sulfoximine **13** in high yield[61]. Corresponding sulfone **14** was obtained from **5a** by further oxidation with *m*CPBA. Besides, the deprotection of the *N*-Boc group occurred smoothly upon the treatment of **7a** with trifluoroacetic acid, affording **15** in 80% yield. The free NH group in **15** offered flexible handles for further functional group elaboration. In the presence of trifluoroacetic anhydride and Et_3N, *N*-protection of **15** with $COCF_3$ delivered compound **16** in 83% yield. X-ray structures of products **12**, **12'**, **14**, **15**, and **16** were presented to confirm the configuration of these products (CCDC: 2468285–2468289).

In conclusion, we have developed an efficient visible-light photocatalytic strategy for the direct construction of angularly fused tetracyclic scaffolds via intermolecular dearomatization of benzothiophene/indole derivatives with cyclopropylamines. This transformation proceeds through a mechanistically distinct cascade involving a photocatalytic dearomative [3+2] cycloaddition followed by cyclization, offering a streamlined approach to structurally complex polycyclic systems. The present work not only expands the synthetic utility of photocatalytic intermolecular dearomative cycloadditions but also provides direct access to structurally distinct angularly fused tetracyclic cores, which are privileged motifs in bioactive molecules. This methodology thus opens an avenue for the rapid assembly of rigid polycyclic architectures with potential applications in medicinal chemistry and natural product synthesis.

Methods

General procedures for the synthesis of product 5. To an oven-dried 4 mL vial with a PTFE-coated stirring bar was added **1** (0.30 mmol, 1.5 eq.), **2** (0.20 mmol, 1.0 eq.), **PC-I** (0.002 mmol, 1 mol%), and acetone (2.0 mL, 0.1 M) in the nitrogen glove box. The vial was capped with a septum and wrapped with parafilm. The reaction mixture was stirred under irradiation with a light box at room temperature for the initial 20–30 h. The reaction mixture was concentrated in vacuo and purified by column chromatography on silica gel using petroleum ether and ethyl acetate to afford the corresponding products.

General procedures for the synthesis of product 7. To an oven-dried 4 mL vial with a PTFE-coated stirring bar was

added **6** (0.20 mmol, 1.0 eq.), **2** (0.30 mmol, 1.5 eq.), Et_3N (0.40 mmol, 2.0 eq.), **PC-I** (0.002 mmol, 1 mol%), and acetone (2.0 mL, 0.1 M) in the nitrogen glove box. The vial was capped with a septum and wrapped with parafilm. The reaction mixture was stirred under irradiation with a light box at room temperature for the initial 20 h. The reaction mixture was concentrated in vacuo, then DBU (0.30 mmol, 1.5 eq.) and acetone (1.0 mL, 0.2 M) were added in the nitrogen glove box. The reaction mixture was stirred at 60 ºC for 6 h. The reaction mixture was concentrated in vacuo and purified by column chromatography on silica gel using petroleum ether and ethyl acetate to afford the corresponding products.

Data availability

The X-ray crystallographic data for compounds generated in this study have been deposited in the Cambridge Crystallographic Data Centre (CCDC), under deposition numbers CCDC 2526038 (**3a**), 2526039 (**3c**), 2526040 (**4a'**), 2526041 (**4d'**), 2468280 (**5a**), 2468281 (**5ab**), 2526042 (**5ad**), 2468282 (**5af**), 2468283 (**7c**), 2526043 (**7g'**), 2468284 (**7aa**), 2526044 (**8a**), 2473229 (**10**), 2473230 (**10'**), 2473231 (**11**), 2468285 (**12**), 2468286 (**12'**), 2468287 (**14**), 2468288 (**15**), and 2468289 (**16**). These data can be obtained free of charge from The Cambridge Crystallographic Data Centre via www.ccdc.cam.ac.uk/data_request/cif. Data relating to the characterization data of materials and products, general methods, optimization studies, experimental procedures, mechanistic studies, mass spectrometry, and NMR spectra are available in the Supplementary Information. All data is available from the corresponding author upon request. The source data generated in this study are provided as a Source Data file.

References

1. Mehta, G. Synthesis of Polyquinane Natural Products: An Update. *Chem. Rev.* **97**, 671–719 (1997).
2. Winkler, J. D. & Jeon, H. Synthesis of Cyclohexane-Angularly-Fused Triquinanes. *Synthesis* **53**, 475–488 (2020).
3. VALDES, F. & ORREGO, F. Strychnine inhibits the Binding of Glycine to Rat Brain-Cortex Membrane. *Nature* **226**, 761–762 (1970).
4. Huang, X., Chen, H., Michelsen, K., Schneider, S. & Shaffer, P. L. Crystal Structure of Human Glycine Receptor-α3 Bound to Antagonist Strychnine. *Nature* **526**, 277–280 (2015).
5. Ma, H., Xie, X., Jing, P., Zhang, W. & She, X. Concise Total Synthesis of (±)-Aspidospermidine. *Org. Biomol. Chem.* **13**, 5255–5259 (2015).
6. Kariba, R. M., Houghton, P. J. & Yenesew, A. Antimicrobial Activities of a New Schizozygane Indoline Alkaloid from Schizozygia coffaeoides and the Revised Structure of Isoschizogaline. *J. Nat. Prod.* **65**, 566–569 (2002).
7. Zhu, X.-X. *et al.* Alstonlarsines A–D, Four Rearranged Indole Alkaloids from Alstonia scholaris. *Org. Lett.* **21**, 1471–1474 (2019).

8. Kärkäs, M. D., Porco, J. A. & Stephenson, C. R. J. Photochemical Approaches to Complex Chemotypes: Applications in Natural Product Synthesis. *Chem. Rev.* **116**, 9683–9747 (2016).

9. Poplata, S., Tröster, A., Zou, Y.-Q. & Bach, T. Recent Advances in the Synthesis of Cyclobutanes by Olefin [2 + 2] Photocycloaddition Reactions. *Chem. Rev.* **116**, 9748–9815 (2016).

10. Remy, R. & Bochet, C. G. Arene–Alkene Cycloaddition. *Chem. Rev.* **116**, 9816–9849 (2016).

11. Sarkar, D., Bera, N. & Ghosh, S. [2+2] Photochemical Cycloaddition in Organic Synthesis. *Eur. J. Org. Chem.* **2020**, 1310–1326 (2020).

12. Sicignano, M., Rodríguez, R. I. & Alemán, J. Recent Visible Light and Metal Free Strategies in [2+2] and [4+2] Photocycloadditions. *Eur. J. Org. Chem.* **2021**, 3303–3321 (2021).

13. Zhu, M., Zhang, X., Zheng, C. & You, S.-L. Energy-Transfer-Enabled Dearomative Cycloaddition Reactions of Indoles/Pyrroles via Excited-State Aromatics. *Acc. Chem. Res.* **55**, 2510–2525 (2022).

14. Hou, L. *et al.* Catalytic Asymmetric Dearomative [2 + 2] Photocycloaddition/Ring-Expansion Sequence of Indoles with Diversified Alkenes. *J. Am. Chem. Soc.* **146**, 23457–23466 (2024).

15. Tian, D. *et al.* Catalytic Asymmetric [4 + 2] Dearomative Photocycloadditions of Anthracene and Its Derivatives with Alkenylazaarenes. *Nat. Commun.* **15**, 4563 (2024).

16. Yang, J. *et al.* Asymmetric Dearomative [2 + 2] Photocycloaddition of Quinoline and Indole Derivatives with Bicyclo[1.1.0]butanes. *J. Am. Chem. Soc.* **147**, 35755–35766 (2025).

17. James, M. J., Schwarz, J. L., Strieth-Kalthoff, F., Wibbeling, B. & Glorius, F. Dearomative Cascade Photocatalysis: Divergent Synthesis through Catalyst Selective Energy Transfer. *J. Am. Chem. Soc.* **140**, 8624–8628 (2018).

18. Ma, J. *et al.* Direct Dearomatization of Pyridines via an Energy-Transfer-Catalyzed Intramolecular [4+2] Cycloaddition. *Chem* **5**, 2854–2864 (2019).

19. Strieth-Kalthoff, F. *et al.* Discovery of Unforeseen Energy-Transfer-Based Transformations Using a Combined Screening Approach. *Chem* **5**, 2183–2194 (2019).

20. Ma, J. *et al.* Gadolinium Photocatalysis: Dearomative [2+2] Cycloaddition/Ring-Expansion Sequence with Indoles. *Angew. Chem. Int. Ed.* **59**, 9639–9645 (2020).

21. Ma, J. *et al.* Photochemical Intermolecular Dearomative Cycloaddition of Bicyclic Azaarenes with Alkenes. *Science* **371**, 1338–1345 (2021).

22. Guo, R. *et al.* Photochemical Dearomative Cycloadditions of Quinolines and Alkenes: Scope and Mechanism Studies. *J. Am. Chem. Soc.* **144**, 17680–17691 (2022).

23. Ma, J. *et al.* Facile Access to Fused 2D/3D Rings via Intermolecular Cascade Dearomative [2 + 2] Cycloaddition/Rearrangement Reactions of Quinolines with Alkenes. *Nat. Catal.* **5**, 405–413 (2022).

24. Kleinmans, R. *et al. ortho*-Selective Dearomative [2π + 2σ] Photocycloadditions of Bicyclic Aza-Arenes. *J. Am. Chem. Soc.* **145**, 12324–12332 (2023).

25. Stegbauer, S., Jandl, C. & Bach, T. Enantioselective Lewis Acid Catalyzed *ortho* Photocycloaddition of Olefins to Phenanthrene-9-carboxaldehydes. *Angew. Chem. Int. Ed.* **57**, 14593–14596 (2018).

26. Zech, A., Jandl, C. & Bach, T. Concise Access to the Skeleton of Protoilludane Sesquiterpenes through a Photochemical Reaction Cascade: Total Synthesis of Atlanticone C. *Angew. Chem. Int. Ed.* **58**, 14629–14632 (2019).

27. Næsborg, L., Jandl, C., Zech, A. & Bach, T. Complex Carbocyclic Skeletons from Aryl Ketones through a Three-Photon Cascade Reaction. *Angew. Chem. Int. Ed.* **59**, 5656–5659 (2020).

28. Yan, P. *et al.* Enantioselective Intramolecular *ortho* Photocycloaddition Reactions of 2-Acetonaphthones. *Angew. Chem. Int. Ed.* **63**, e202318126 (2024).

29. Hu, N. *et al.* Catalytic Asymmetric Dearomatization by Visible-Light-Activated [2+2] Photocycloaddition. *Angew. Chem. Int. Ed.* **57**, 6242–6246 (2018).

30. Zhu, M., Zheng, C., Zhang, X. & You, S.-L. Synthesis of Cyclobutane-Fused Angular Tetracyclic Spiroindolines via Visible-Light-Promoted Intramolecular Dearomatization of Indole Derivatives. *J. Am. Chem. Soc.* **141**, 2636–2644 (2019).

31. Zhu, M., Zhang, X., Zheng, C. & You, S.-L. Visible-Light-Induced Dearomatization via [2+2] Cycloaddition or 1,5-Hydrogen Atom Transfer: Divergent Reaction Pathways of Transient Diradicals. *ACS Catal.* **10**, 12618–12626 (2020).

32. Zhu, M., Huang, X.-L., Sun, S., Zheng, C. & You, S.-L. Visible-Light-Induced Dearomatization of Indoles/Pyrroles with Vinylcyclopropanes: Expedient Synthesis of Structurally Diverse Polycyclic Indolines/Pyrrolines. *J. Am. Chem. Soc.* **143**, 13441–13449 (2021).

33. Zhu, M., Xu, H., Zhang, X., Zheng, C. & You, S. L. Visible-Light-Induced Intramolecular Double Dearomative Cycloaddition of Arenes. *Angew. Chem. Int. Ed.* **60**, 7036–7040 (2021).

34. Oderinde, M. S. *et al.* Synthesis of Cyclobutane-Fused Tetracyclic Scaffolds via Visible-Light Photocatalysis for Building Molecular Complexity. *J. Am. Chem. Soc.* **142**, 3094–3103 (2020).

35. Arai, N. & Ohkuma, T. Stereoselective Construction of Methylenecyclobutane-Fused Indolines through Photosensitized [2+2] Cycloaddition of Allene-Tethered Indole Derivatives. *Org. Lett.* **21**, 1506–1510 (2019).

36. Arai, N. & Ohkuma, T. Photosensitized Intramolecular [2+2] Cycloaddition of 1*H*-Pyrrolo[2,3-*b*]pyridines Enabled by the Assistance of Lewis Acids. *J. Org. Chem.* **85**, 15717–15725 (2020).

37. Zhang, Z. *et al.* Photocatalytic Intramolecular [2 + 2] Cycloaddition of Indole Derivatives via Energy Transfer: A Method for Late-Stage Skeletal Transformation. *ACS Catal.* **10**, 10149–10156 (2020).

38. Li, H. *et al.* Hydrogen Bond Serving as a Protecting Group to Enable the Photocatalytic [2+2] Cycloaddition of

Redox-Active Aliphatic-Amine-Containing Indole Derivatives. *Chem. Commun.* **58**, 3194–3197 (2022).

39. Sauvé, E. R., Mayder, D. M., Kamal, S., Oderinde, M. S. & Hudson, Z. M. An Imidazoacridine-Based TADF Material as an Effective Organic Photosensitizer for Visible-Light-Promoted [2 + 2] Cycloaddition. *Chem. Sci.* **13**, 2296–2302 (2022).
40. Mu, X. P. *et al.* Stereoselective Synthesis of Cyclohepta[*b*]indoles by Visible-Light-Induced [2+2]-Cycloaddition/retro-Mannich-type Reactions. *Angew. Chem. Int. Ed.* **60**, 11211–11216 (2021).
41. Morris, S. A., Wang, J. & Zheng, N. The Prowess of Photogenerated Amine Radical Cations in Cascade Reactions: From Carbocycles to Heterocycles. *Acc. Chem. Res.* **49**, 1957–1968 (2016).
42. Harmata, A. S., Roldan, B. J. & Stephenson, C. R. J. Formal Cycloadditions Driven by the Homolytic Opening of Strained, Saturated Ring Systems. *Angew. Chem. Int. Ed.* **62**, e202213003 (2023).
43. Wang, M.-M., Nguyen, T. V. T. & Waser, J. Activation of Aminocyclopropanes via Radical Intermediates. *Chem. Soc. Rev.* **51**, 7344–7357 (2022).
44. Maity, S., Zhu, M., Shinabery, R. S. & Zheng, N. Intermolecular [3+2] Cycloaddition of Cyclopropylamines with Olefins by Visible-Light Photocatalysis. *Angew. Chem. Int. Ed.* **51**, 222–226 (2011).
45. Cai, Y. *et al.* Detection of Fleeting Amine Radical Cations and Elucidation of Chain Processes in Visible-Light-Mediated [3 + 2] Annulation by Online Mass Spectrometric Techniques. *J. Am. Chem. Soc.* **139**, 12259–12266 (2017).
46. Kuang, Y., Ning, Y., Zhu, J. & Wang, Y. Dirhodium(II)-Catalyzed (3 + 2) Cycloaddition of the *N*-Arylaminocyclopropane with Alkene Derivatives. *Org. Lett.* **20**, 2693–2697 (2018).
47. Muriel, B., Gagnebin, A. & Waser, J. Synthesis of Bicyclo[3.1.0]hexanes by (3 + 2) Annulation of Cyclopropenes with Aminocyclopropanes. *Chem. Sci.* **10**, 10716–10722 (2019).
48. Yin, Y. *et al.* All-Carbon Quaternary Stereocenters *α* to Azaarenes via Radical-Based Asymmetric Olefin Difunctionalization. *J. Am. Chem. Soc.* **142**, 19451–19456 (2020).
49. Luo, Z. *et al.* Visible-Light Organophotoredox-Mediated [3 + 2] Cycloaddition of Arylcyclopropylamine with Structurally Diverse Olefins for the Construction of Cyclopentylamines and Spiro[4.*n*] Skeletons. *J. Org. Chem.* **87**, 15511–15529 (2022).
50. Feng, D., Geng, X., Zuo, L., Li, Z. & Wang, L. Radical-Polar Crossover Bicyclization Enables a Modular Synthesis of Saturated Bicyclic Amines. *Adv. Sci.* **12**, 2501310 (2025).
51. Wang, J., Nguyen, T. H. & Zheng, N. Photoredox-Catalyzed [4+2] Annulation of Cyclobutylanilines with Alkenes, Alkynes, and Diynes in Continuous Flow. *Sci. China Chem.* **59**, 180–183 (2016).
52. Wang, J., Mao, C., Feng, P. & Zheng, N. Visible-Light-Mediated [4+2] Annulation of *N*-Cyclobutylanilines with Alkynes Catalyzed by Self-Doped Ti^{3+}@TiO_2. *Chem. Eur. J.* **23**, 15396–15403 (2017).

53. Zheng, Y. *et al.* Photochemical Intermolecular [3*σ* + 2*σ*]-Cycloaddition for the Construction of Aminobicyclo[3.1.1]heptanes. *J. Am. Chem. Soc.* **144**, 23685–23690 (2022).

54. Song, T.-T. *et al.* Construction of Bridged Benzazepines via Photo-Induced Dearomatization. *Angew. Chem. Int. Ed.* **63**, e202314304 (2024).

55. Zhang, X.-X. *et al.* Dearomative Skeletal Editing of Benzenoids via Diradical. *J. Am. Chem. Soc.* **147**, 11533–11542 (2025).

56. Song, T.-T. *et al.* Divergent Construction of Cyclobutane-Fused Pentacyclic Scaffolds via Double Dearomative Photocycloaddition. *Angew. Chem. Int. Ed.* **64**, e202505906 (2025).

57. Lin, F. *et al.* Photo-Induced Catalytic Dearomative Coupling of *N*-Heteroarenes. *Angew. Chem. Int. Ed.* **64**, e202513552 (2025).

58. White, D. H., Noble, A., Booker-Milburn, K. I. & Aggarwal, V. K. Diastereoselective Photoredox-Catalyzed [3 + 2] Cycloadditions of N-Sulfonyl Cyclopropylamines with Electron-Deficient Olefins. *Org. Lett.* **23**, 3038–3042 (2021).

59. Uraguchi, D., Kimura, Y., Ueoka, F. & Ooi, T. Urea as a Redox-Active Directing Group under Asymmetric Photocatalysis of Iridium-Chiral Borate Ion Pairs. *J. Am. Chem. Soc.* **142**, 19462–19467 (2020).

60. Prier, C. K., Rankic, D. A. & MacMillan, D. W. C. Visible Light Photoredox Catalysis with Transition Metal Complexes: Applications in Organic Synthesis. *Chem. Rev.* **113**, 5322–5363 (2013).

61. Zenzola, M., Doran, R., Degennaro, L., Luisi, R. & Bull, J. A. Transfer of Electrophilic NH Using Convenient Sources of Ammonia: Direct Synthesis of NH Sulfoximines from Sulfoxides. *Angew. Chem. Int. Ed.* **55**, 7203–7207 (2016).

Acknowledgements

We thank Prof. Zhi-Shi Ye (DUT) for helpful discussions and manuscript revisions.

Funding

Financial support from the National Natural Science Foundation of China (22501278, T.-T.S) is acknowledged.

Author contributions

Q.-A.C., Y.S., and T.-T.S. conceived and supervised the project. Q.-A.C., T.-T.S., and F.L. designed the experiments. F.L., T.-T.S., L.-M.Z., Z.-Y.D., Y.J., Y.L., and B.W. performed the experiments and analyzed the data. All authors discussed the results and commented on the manuscript.

Competing interests

The authors declare no competing interests.

Tables

Table 1. Optimization of the reaction conditions[a]

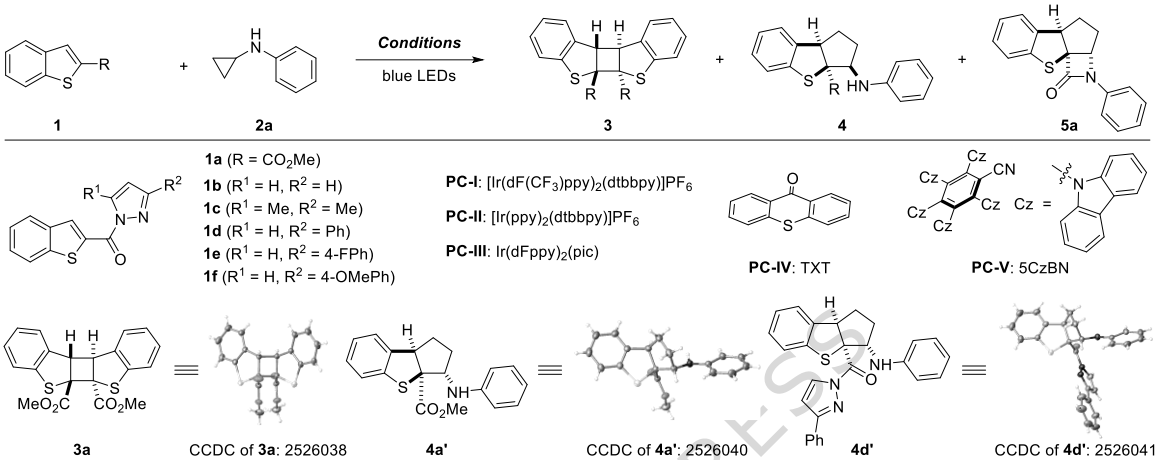

Entry	**1**	Solvent	Photocatalyst	**3** (%)[b] (dr)	**4** (%)[b] (dr)	**5a** (%)[b]
1	**1a**	Acetone	PC-I	63 (> 95:5)	50 (67:33)	N.D.
2	**1a**	THF	PC-I	43 (> 95:5)	16 (70:30)	N.D.
3	**1a**	DCM	PC-I	74 (> 95:5)	6 (62:38)	N.D.
4	**1a**	Acetone	PC-II	51 (> 95:5)	30 (67:33)	N.D.
5	**1a**	Acetone	PC-III	53 (> 95:5)	22 (75:25)	N.D.
6	**1a**	Acetone	PC-IV[c]	82 (> 95:5)	10 (67:33)	N.D.
7	**1a**	Acetone	PC-V	85 (> 95:5)	2 (57:43)	N.D.
8	**1b**	Acetone	PC-I	35 (> 95:5)	< 5	67
9	**1c**	Acetone	PC-I	20 (> 95:5)	< 5	61
10	**1d**	Acetone	PC-I	11 (> 95:5)	< 5	74 (71)[e]
11	**1e**	Acetone	PC-I	23 (> 95:5)	< 5	57
12	**1f**	Acetone	PC-I	18 (> 95:5)	< 5	66
13	**1d**	DMSO	PC-I	6 (> 95:5)	39 (< 5:95)	24
14	**1d**	$MeNO_2$	PC-I	22 (> 95:5)	12 (< 5:95)	Trace
15	**1d**	Acetone	none	0	0	0
16[d]	**1d**	Acetone	PC-I	0	0	0

[a]Reaction conditions: **1** (0.15 mmol), **2a** (0.10 mmol), and photocatalyst (1 mol%), solvent (1.0 mL), blue LEDs, RT, 20 h. [b]Yields were determined by GC-FID. Yield of **3** was calculated based on substrate **1** (0.15 mmol). [c]Photocatalyst (5 mol%). [d]In the absence of light irradiation. [e]Isolated yield.

Figure Legends/Captions (For Main Text Figures)

Fig. 1 Intermolecular dearomative cycloaddition for constructing angularly fused tetracyclic scaffolds. a Representative natural polycyclic scaffolds molecules. **b** Previous work: Construction of angularly fused tetracyclic scaffolds via intramolecular dearomatization. **c** The reaction pattern of CPAs in photochemical reactions. **d**, Design plan: Intermolecular dearomatization. **e** This work: Visible light-induced intermolecular dearomatization for constructing angularly fused tetracyclic scaffolds.

Fig. 2 Substrate scope of benzothiophene derivatives. Conditions: **1** (0.30 mmol), **2** (0.20 mmol), and **PC-I** (1 mol%), acetone (2 mL), blue LEDs (24 W), RT, 20 h. [a]**1** (0.20 mmol) and **2** (0.20 mmol) were used. Isolated yields were given.

Fig. 3 The substrate scope of indole derivatives and one-pot substrate scope. a The substrate scope of indole derivatives. Conditions: I) **6** (0.20 mmol), **2** (0.30 mmol), and **PC-I** (1 mol%), Et_3N (2.0 eq.), acetone (2.0 mL), blue LEDs (24 W), RT, 20 h. II) DBU (2.0 eq.), 60 °C, 6 h. [a]THF was used instead of acetone. [b]Step 2: 390 nm, RT, 16 h. Isolated yields were given. N.D.: Not detected. N.R.: No reaction. **b** One-pot substrate scope. Conditions: I) **1'** (0.40 mmol), 3-phenyl-1H-pyrazole (0.60 mmol), EDCI (0.80 mmol), DMAP (20 mol%), DCM (1.0 mL), RT, 12 h. II) **2** (0.20 mmol), **PC-I** (1 mol%), acetone (1.0 mL), blue LEDs (24 W), RT, 20 h. Isolated yields were given.

Fig. 4 Mechanistic studies. a Investigation of involved intermediates. **b** Kinetic profile. **c** Light on/off experiments. **d** UV-vis absorption analysis. **e** Stern-Volmer quenching studies. **f** Radical inhibition experiments. **g** Diradical capture experiments. **h** The role of adding Et_3N. **i** Intermediate conversion experiments.

Fig. 5 Proposed mechanism.

Fig. 6 Scale-up experiments and synthetic transformations. a Scale-up experiments. **b** Synthetic transformations.

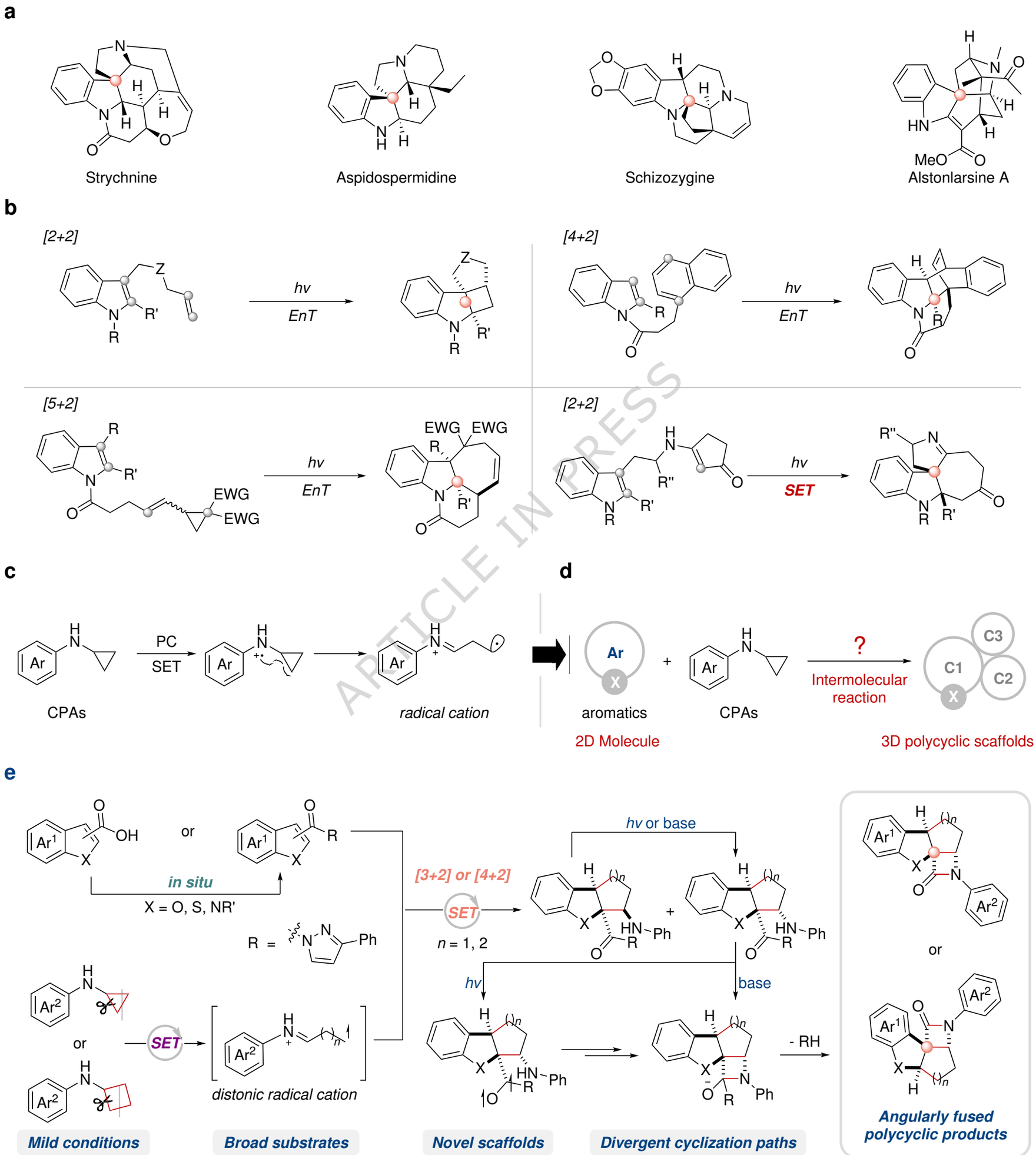

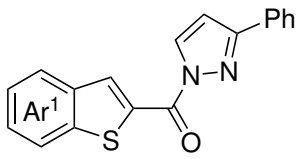

1

+

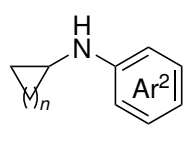

n = 1, 2

2

PC-I (1 mol%)

acetone, blue LEDs, RT, 20 h

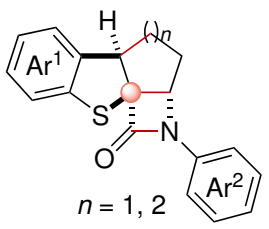

n = 1, 2

5

PC-I

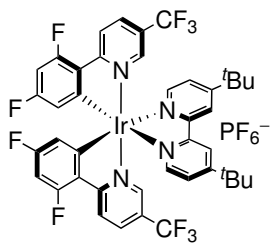

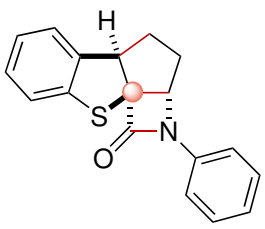

5a, 71%

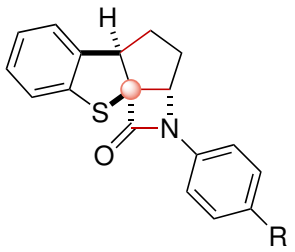

5b (R = Me), 68%
5c (R = *t*Bu), 56%

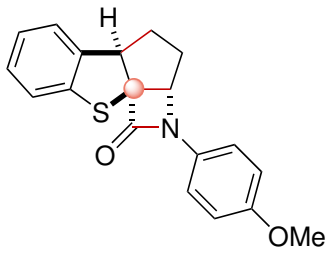

5d, 66%

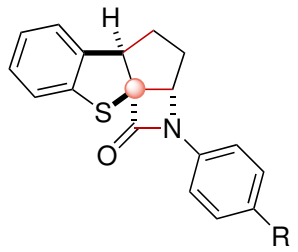

5e (R = F), 70%
5f (R = Cl), 65%

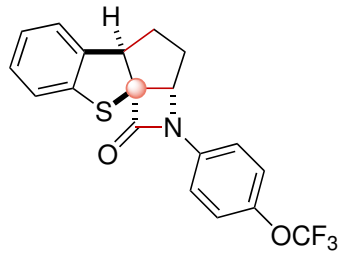

5g, 60%

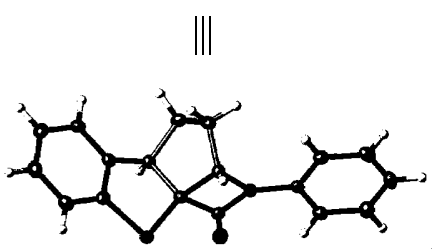

CCDC of **5a**: 2468280

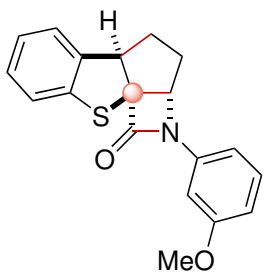

5h, 67%

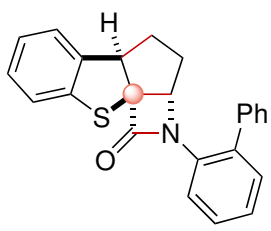

5i, 69%

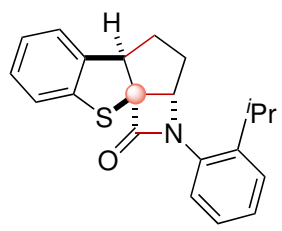

5j, 70%

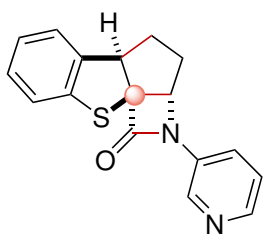

5k, 54%

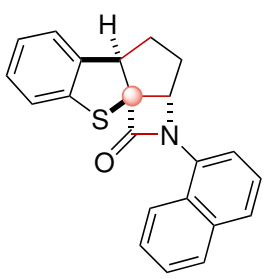

5l, 52%

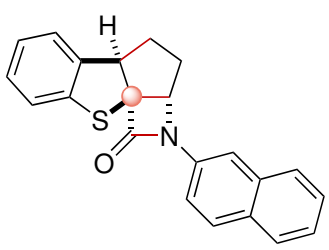

5m, 60%

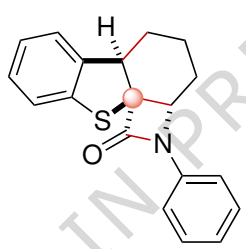

5n, 69%

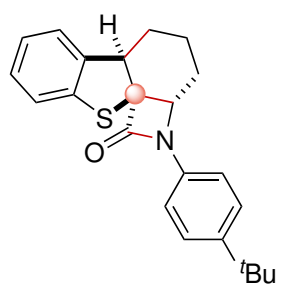

5o, 60%

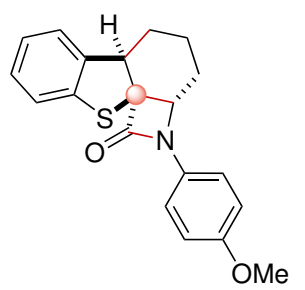

5p, 66%

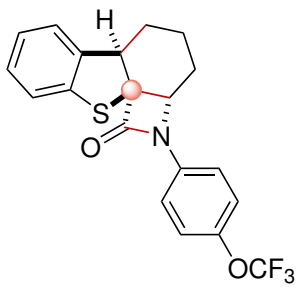

5q, 67%

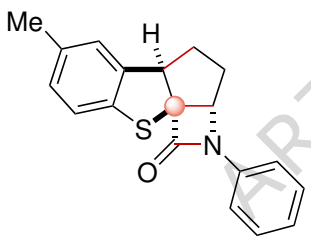

5r, 59%

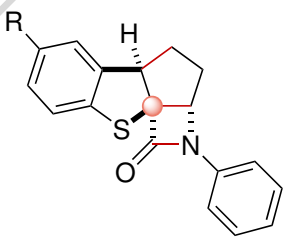

5s (R = F), 60%
5t (R = Cl), 55%

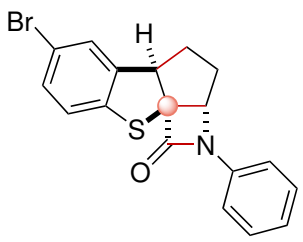

5u, 53%

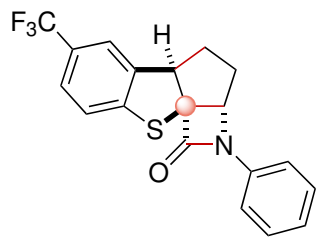

5v, 62%

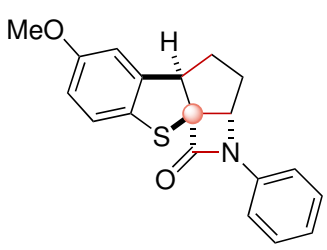

5w, 66%

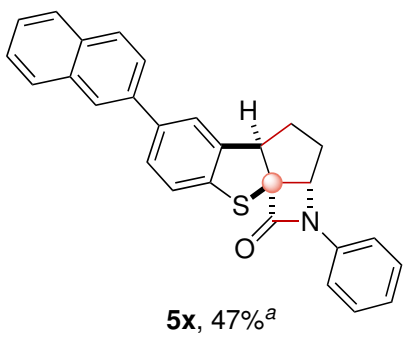

5x, 47%[a]

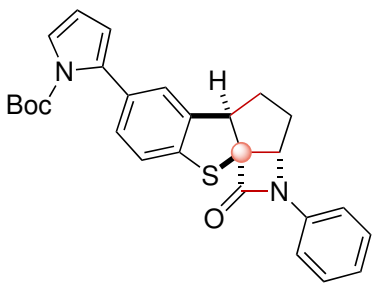

5y, 68%

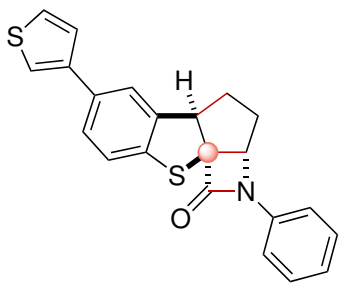

5z, 71%

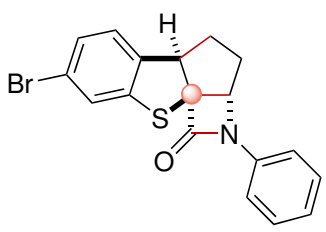

5aa, 53%

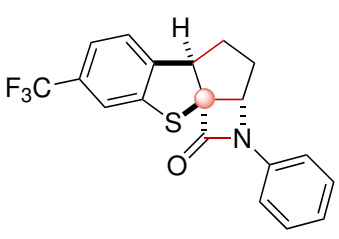

5ab, 65%

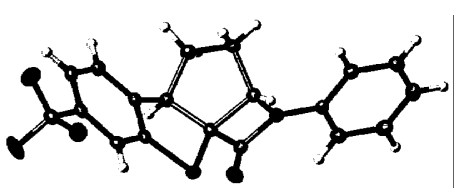

CCDC of **5ab**: 2468281

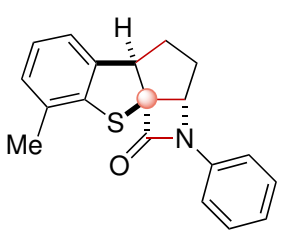

5ac, 58%

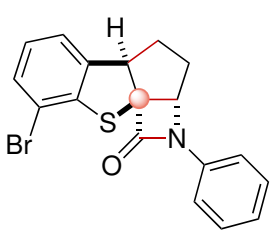

5ad, 61%

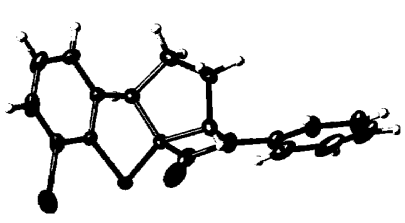

CCDC of **5ad**: 2526042

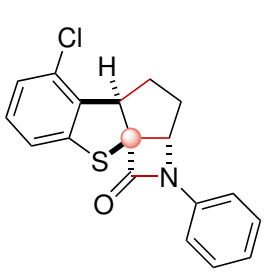

5ae, 50%

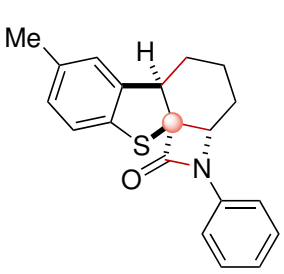

5af, 65%

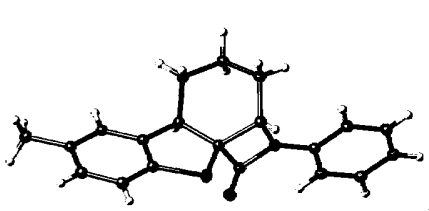

CCDC of **5af**: 2468282

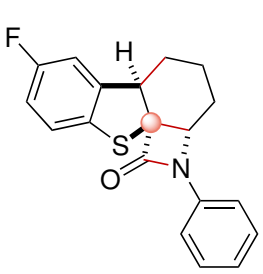

5ag, 60%

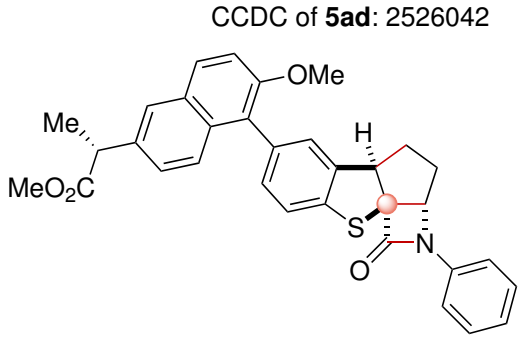

5ah (from Naproxen), 58%,[a] 1:1 dr

a

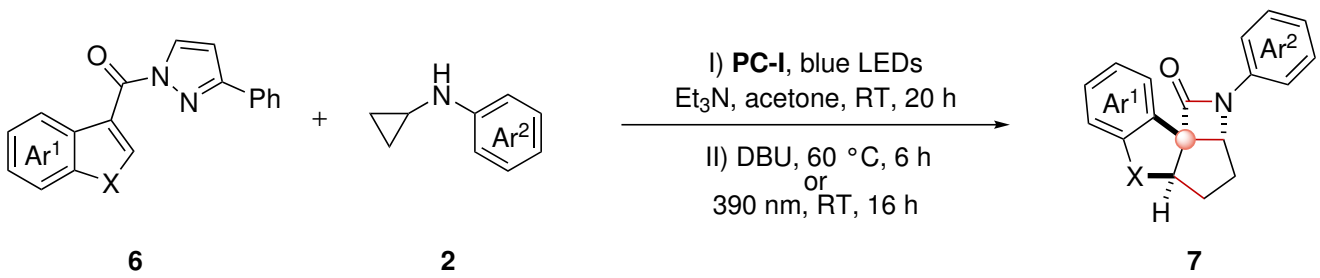

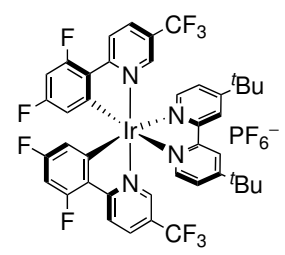

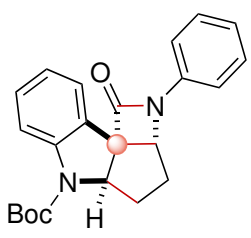

7a, 73%

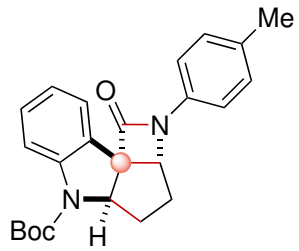

7b, 63%

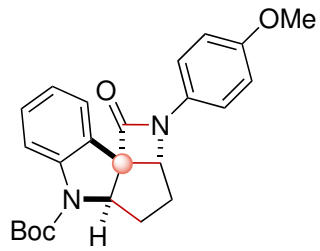

7c, 59%

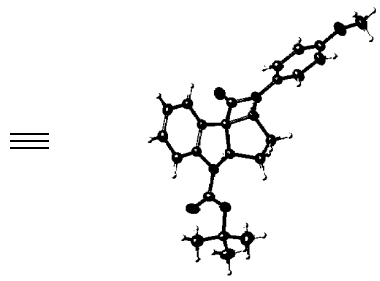

CCDC of **7c**: 2468283

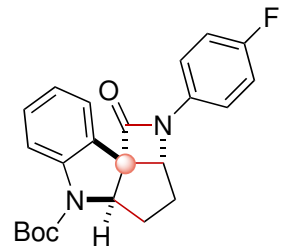

7d, 48%

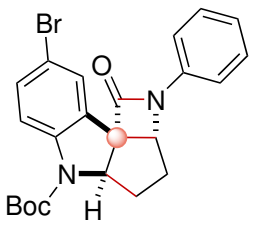

7e, 43%[a]

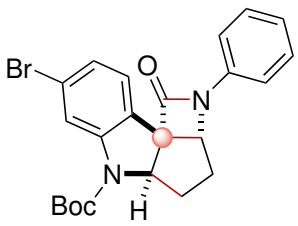

7f, 50%[a,b]

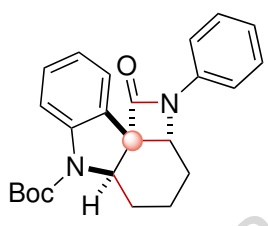

7g, N.D.[a]

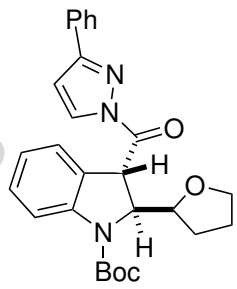

7g', 52%[a]

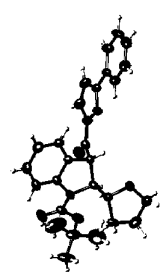

CCDC of **7g'**: 2526043

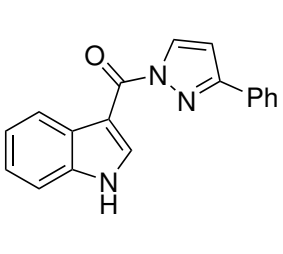

6h, N.R.

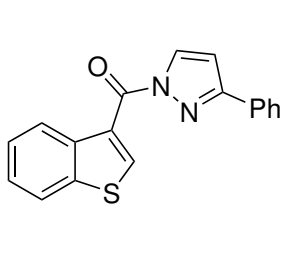

6i

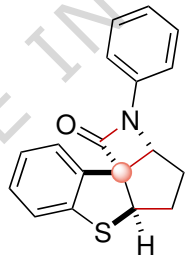

7i, 30%

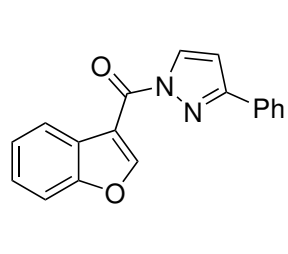

6j

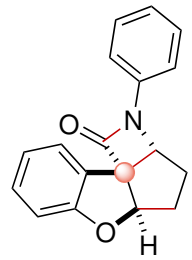

7j, 48%

b

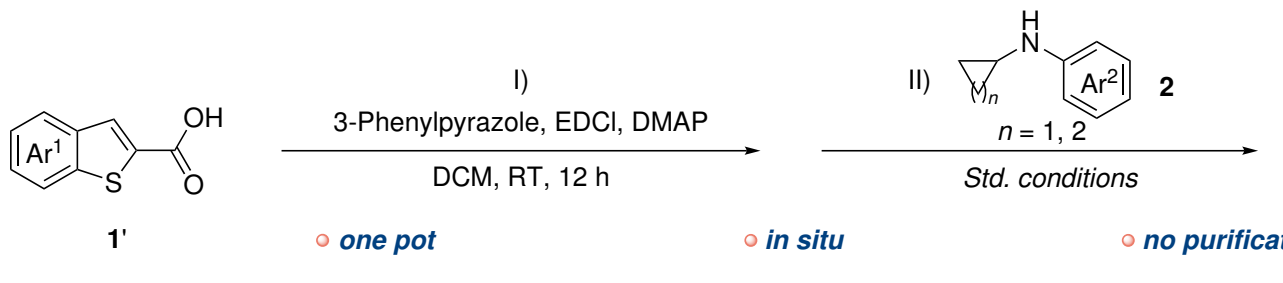

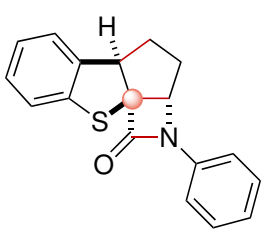

5a, 65%

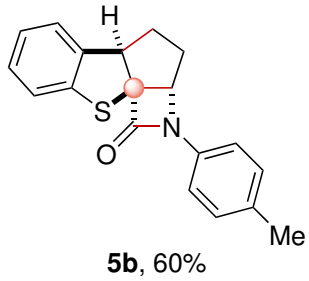

5b, 60%

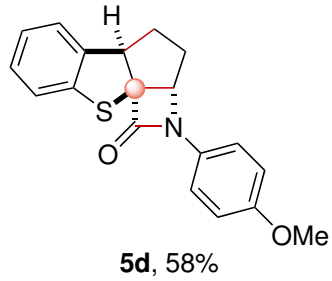

5d, 58%

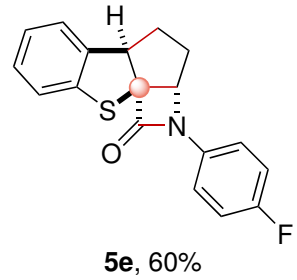

5e, 60%

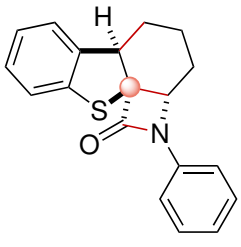

5n, 59%

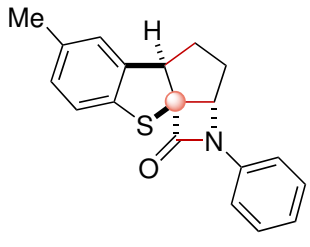

5r, 49%

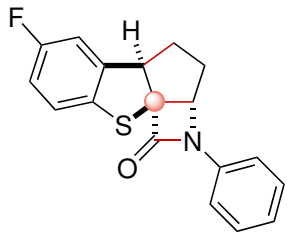

5s, 53%

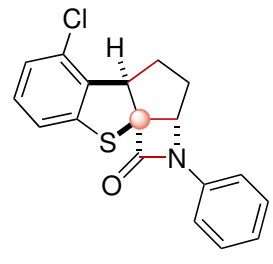

5ae, 45%

a

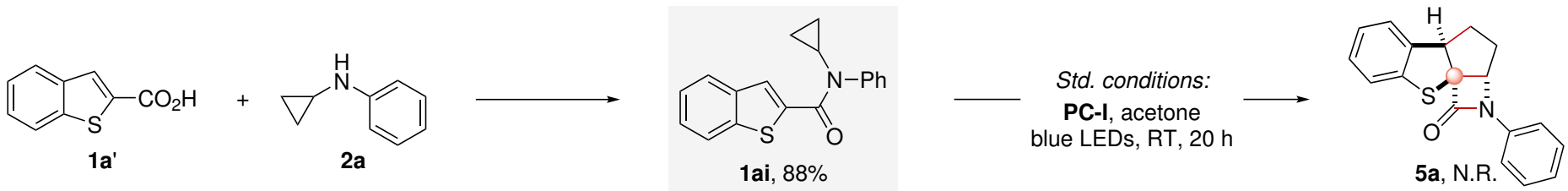

b

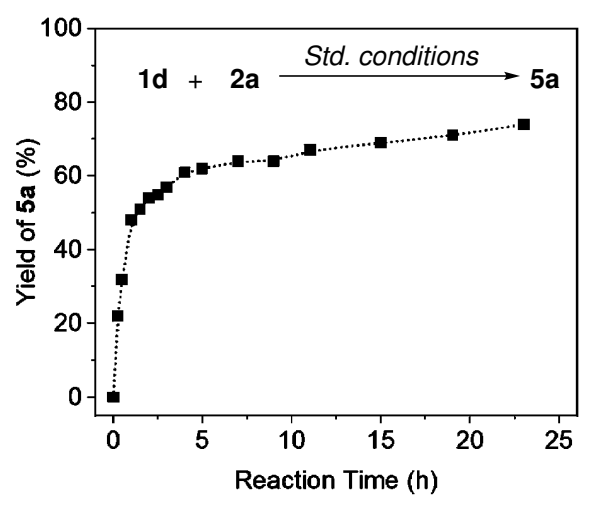

c

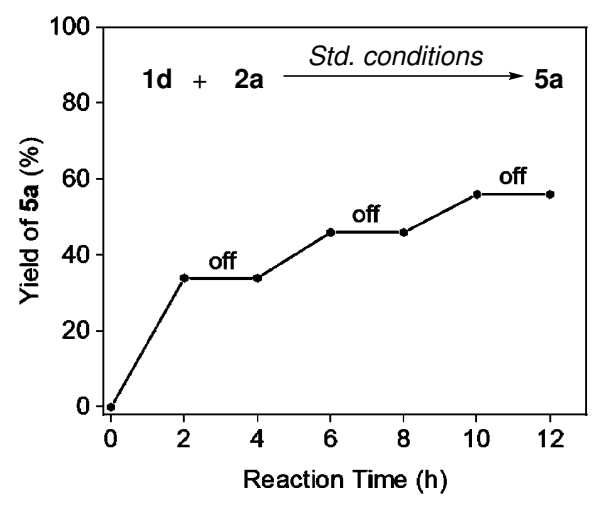

d

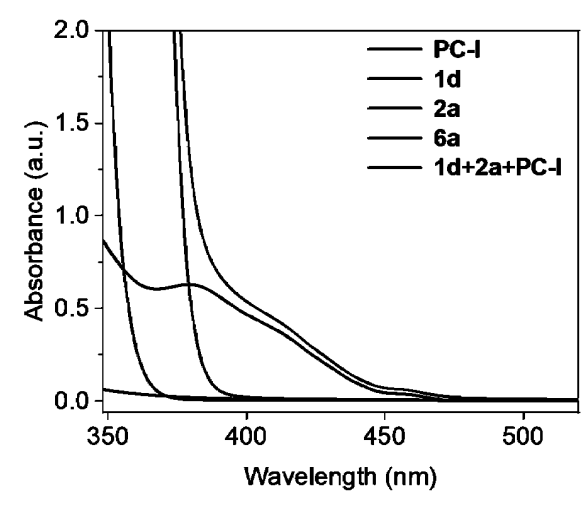

e

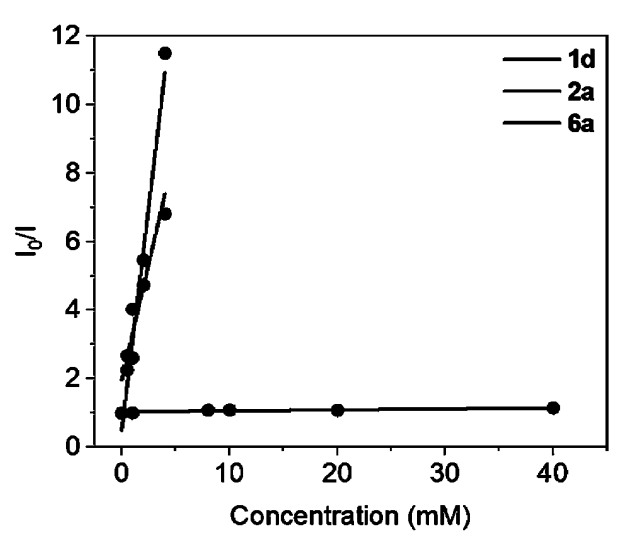

f

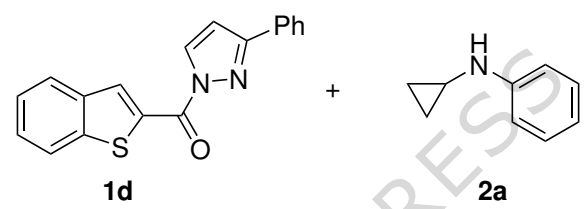

Entry	Additives	Yield of **5a** (%)
1	None	74
2	BHT (3.0 eq.)	43
3	TEMPO (3.0 eq.)	0
4	Air	45
5	1,1-Diphenylethylene	18

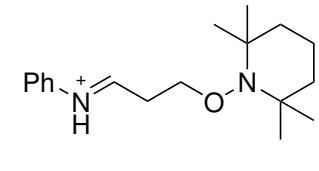

TEMPO-adduct
Deteceted by HRMS

g

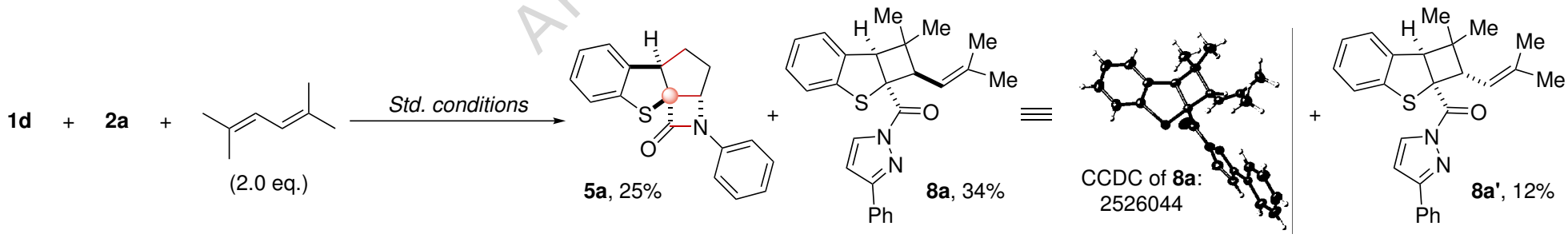

h

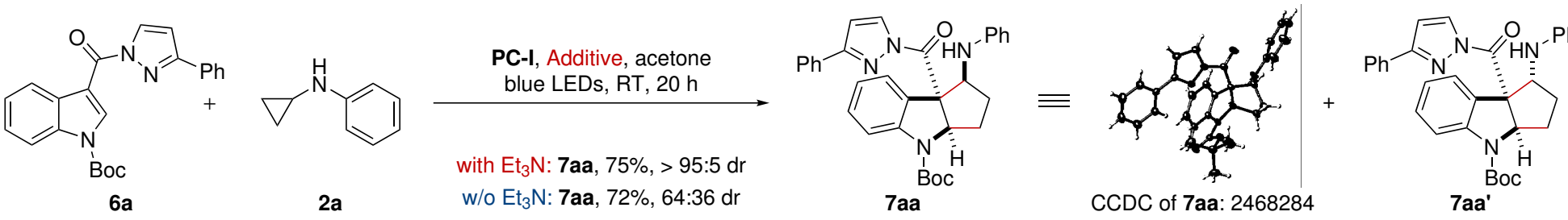

i

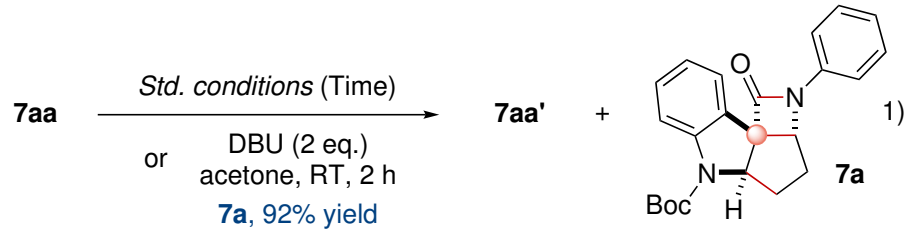

Entry	Time (h)	Yield of **7aa'** (%)	Yield of **7a** (%)
1	1	9	16
2	2	13	24
3	4	14	46
4	8	trace	96

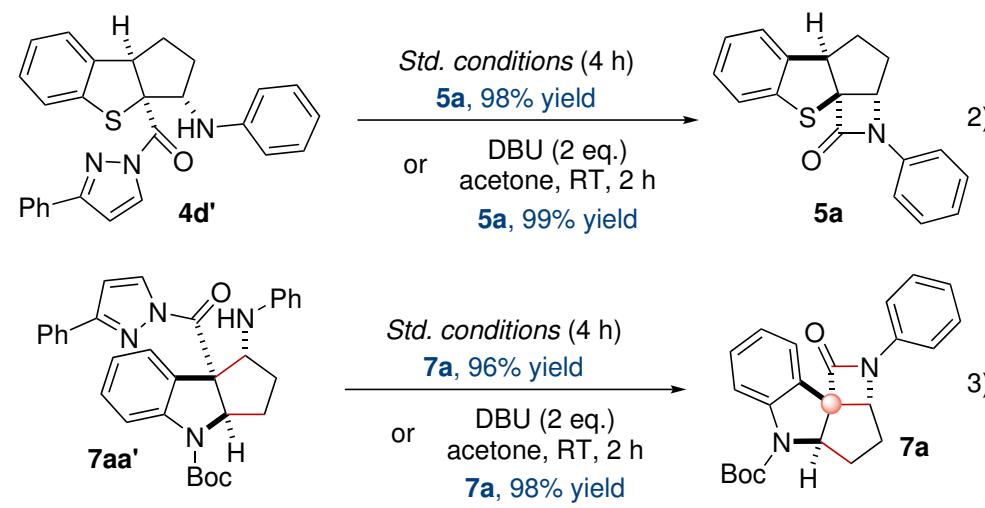

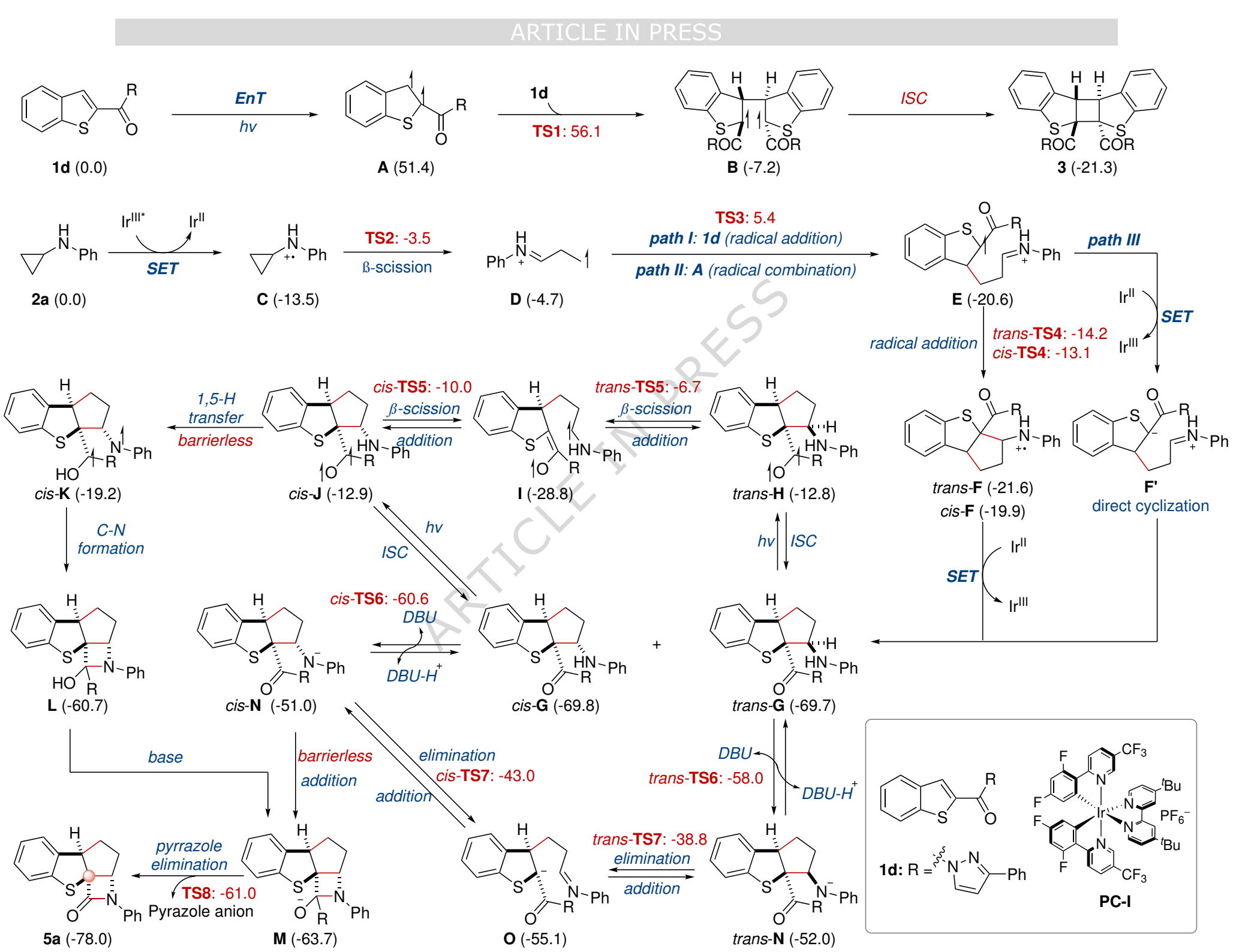

a

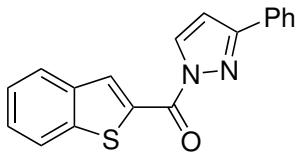

1d

+

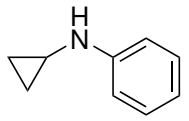

2a, 8.0 mmol

PC-I (1 mol%)

acetone, blue LEDs, RT, 20 h

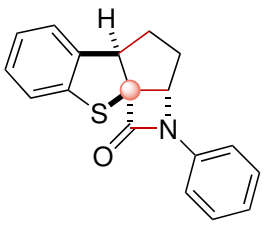

5a, 1.61 g, 69%

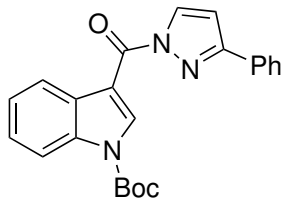

6a, 3.1 mmol

+

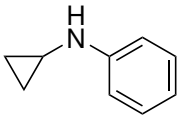

2a

I) **PC-I**, NEt_3, acetone, blue LEDs, RT, 20 h

II) DBU, 60 °C, 6 h

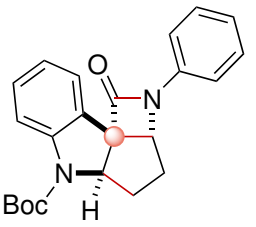

7a, 0.85 g, 73%

b

Redox transformations of **5a**

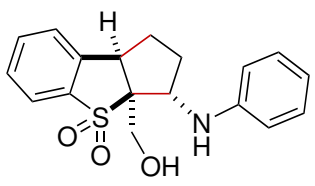

11, 60%

≡

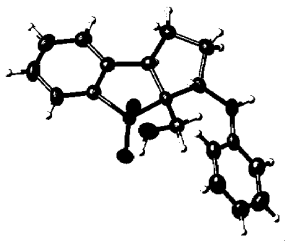

CCDC of **11**: 2473231

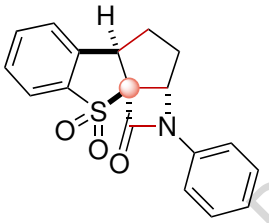

14, 94%

≡

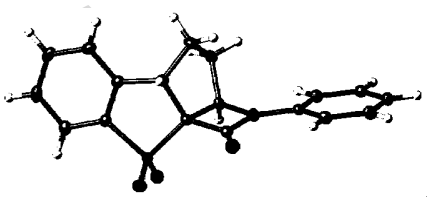

CCDC of **14**: 2468287

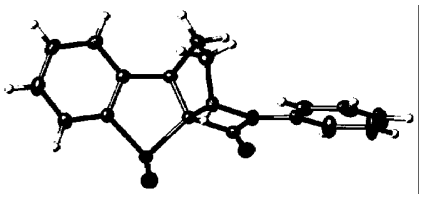

CCDC of **12'**: 2468286

H_2O_2

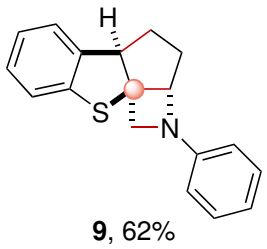

9, 62%

*m*CPBA

LiAlH$_4$

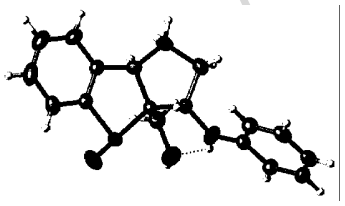

CCDC of **10**: 2473229

*m*CPBA

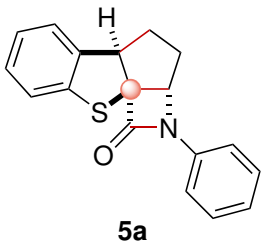

5a

CAN

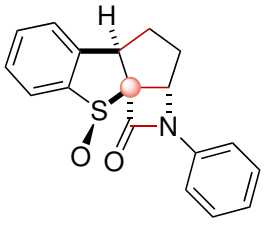

12', 15%

+

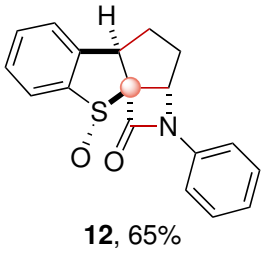

12, 65%

$NH_2CO_2NH_4$

$PhI(OAc)_2$

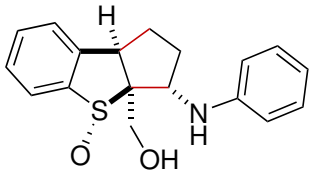

10, 61%

+

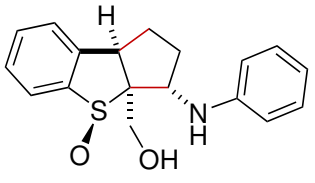

10', 10%

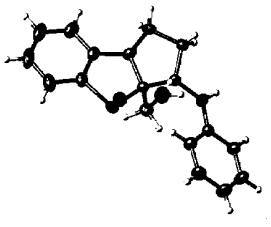

CCDC of **10'**: 2473230

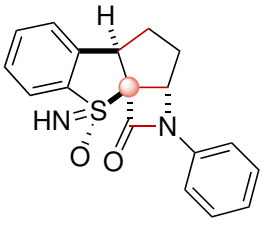

13, 89% (from **12**)

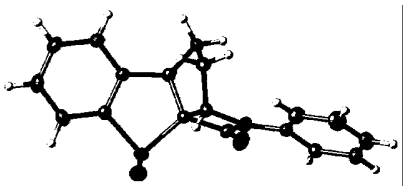

CCDC of **12**: 2468285

Deprotection of *N*-Boc group and *N*-protection with $COCF_3$

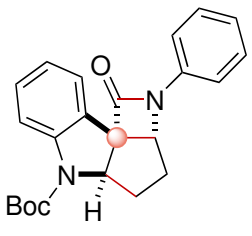

7a

CF_3CO_2H

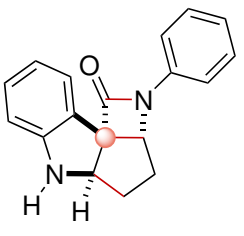

15, 80%

≡

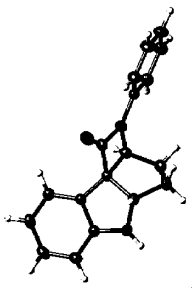

CCDC of **15**: 2468288

$(CF_3CO)_2O$, Et_3N

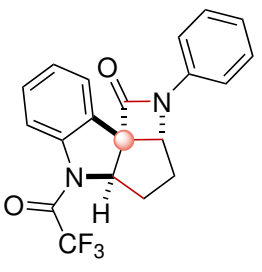

16, 83%

≡

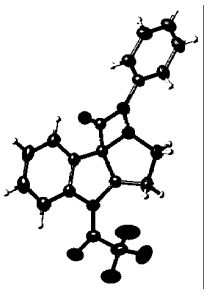

CCDC of **16**: 2468289